J. Membrane Biol. 71, 61–78 (1983)

The Journal of
Membrane Biology

Multioccupancy Models for Single Filing Ionic Channels: Theoretical Behavior of a Four-Site Channel with Three Barriers Separating the Sites

John Sandblom, George Eisenman*, and Jarl Hägglund**

Department of Physiology and Medical Biophysics, University of Uppsala, Uppsala, Sweden

Summary. A procedure is developed for dealing with multioccupancy in single-filing channels having any number of sites internal to the barriers at the channel ends but having the outermost sites in equilibrium with the bathing solutions. Using this procedure, a general theory is developed for a single-filing channel having three barriers and four sites, the outermost of which are in equilibrium with the bathing solutions. By introducing a vectorial representation, it is shown that the four-site model can be reduced to an equivalent two-site model with respect to the number of possible transitions, thereby simplifying the algebraic steps required to solve transport equations for the system. The transport coefficients are derived and expressed in terms of the energy levels of the peaks and the wells for the different occupancy configurations. An explicit solution to the transport equations is given in a comprised form for a single permeable species. The solution allows some important properties for the system to be deduced, specifically with regard to the conductance at zero current, the correlation factor between electrical conductance and tracer flux, and the current-voltage relationship. Examples are given for the use of the present results in a physical interpretation of the data from the gramicidin A channel.

Key Words single-filing channel · barrier model · gramicidin A · multiple occupancy · external sites

Introduction

Accumulating experimental data on ionic channels in biological membranes, as well as in lipid bilayers, has made it apparent that it is possible for a channel to accommodate several interacting ions while at the same time it may be sufficiently narrow to prevent ions (and water molecules) from passing each other as they jump step-wise along a linear sequence of sites (*cf.* Eisenman, Sandblom & Neher, 1978; Hille, 1978; Hille & Schwartz, 1978; Levitt, Elias & Hautman, 1978; Rosenberg & Finkelstein, 1978; Hägglund, Enos & Eisenman, 1979; Urban & Hladky, 1979; Procopio & Andersen, 1979). Although the exact energy profile experienced by an ion traversing even the simplest channel is exceedingly complex, only one or a few steps will actually be rate limiting for a given set of experimental conditions and only the most favorable positions will function as sites. It therefore seems reasonable to represent the movement of an ion by a series of discrete jumps over energy barriers separating a relatively few sites.

The transport equations for these models are generally derived in the way described by Heckmann (1965*a*, *b*; 1968) using Eyring rate theory. Although this involves a great number of rate constants in more complicated situations, it is often possible to lump the parameters into a few experimentally measurable quantities. Such a procedure was developed by Sandblom, Eisenman and Neher (1977) in fitting a single barrier four-site model to the data of the gramicidin A channel. In the present paper we extend this treatment to a more general case of three barriers and four sites, partly because a single-barrier model shows a very restricted behavior with respect to current-voltage relationships and flux ratio exponent, particularly with respect to gramicidin A channels. There are also a number of observations which suggest that two sites are not enough to account for the properties of gramicidin A channels. Foremost of these is the inability of a two-site model to reconcile the flux ratio exponent data for Cs measured by Procopio and Andersen (1979) with the conductance-concentration behavior at high concentrations where the con-

* *Permanent address:* Department of Physiology, UCLA Medical School, Los Angeles, Calif.

** *Permanent address:* Department of Neurology, University Hospital, Uppsala, Sweden.

0022-2631/83/0071-0061 $03.60

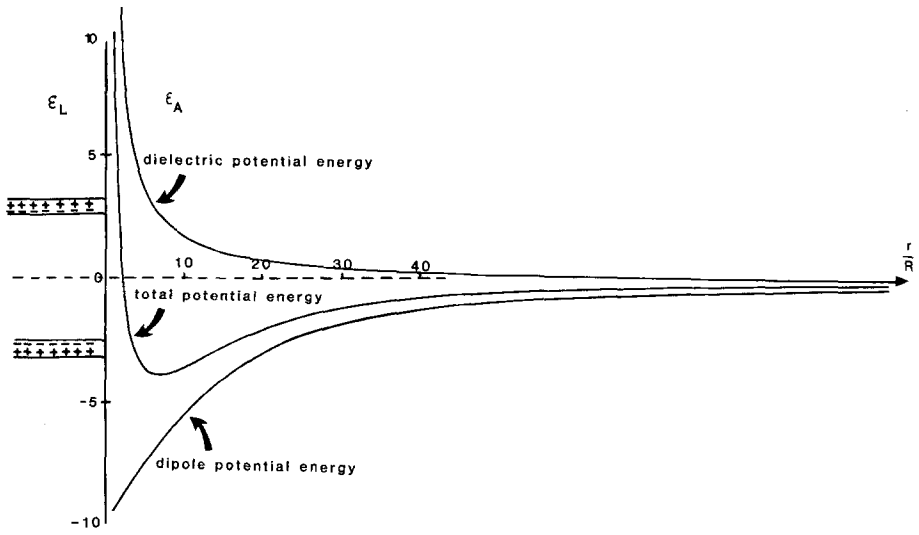

Fig. 1. The different contributions to the total energy for a point charge located at the axis of an infinitely long cylindrical pore lined with dipoles. The distance from the interface is given in units of r/R where R is the pore radius and r the actual distance from the mouth of the pore. The potential energy is plotted along the ordinate in units of kT. By setting $R=1$ Å, $\varepsilon_L=0$, $\varepsilon_A=80 \times \varepsilon_o$ and $p=\frac{1}{2}e$, the image profile energy and the dipole energy have been computed separately according to Eqs. (1) and (2) and plotted here together with the total energy, consisting of the sum of the two terms

ductance passes through a maximum when the flux ratio exponent is still increasing (*cf.* Fig. 9*A* and *B*). In addition, certain complexities in the conductance-concentration behavior for Tl, Ag and H as well as the details of the variation of permeability ratios for Tl-K mixtures (Eisenman et al., 1978) and the *I-V* shape as a function of ion concentration (Eisenman, Hägglund, Sandblom & Enos, 1980; Eisenman, Sandblom & Hägglund, 1982) all suggest that it is necessary to consider the properties of channels occupiable by more than two cations in making an adequate model for the gramicidin channel. The present paper may therefore also be seen as an extension of the three-barrier two-site model (3*B*2*S*) (Hille & Schwarz, 1978; Urban & Hladky, 1979) by the addition of outer sites in equilibrium with the aqueous solutions (3*B*4*S*′)[1].

In studying the properties of this model we will allow all the sites to be occupied simultaneously. Although the electrostatic repulsion energies inside the channel increase considerably when two or more ions occupy the channel (Levitt, 1978), the effects are markedly reduced at the ends of the channel where screening effects from the aqueous solutions become important (Sandblom et al., 1977). From an energetic point of view it is therefore possible to assume the inner sites to be located inside the channel and the outer sites to be located at, or very near, the ends of the channel. Hence whereas binding to the inner sites occurs through interactions with the ligands of the peptide backbone, the binding to outer sites may involve quite different mechanisms, for instance, a competition between image forces and permanent dipoles of the channel to create energy wells at, or even outside, the channel ends.

A simplified physical model of the latter case is shown in Fig. 1. The channel is lined with dipoles and the dielectric constant of the medium is assumed to be uniform. For an infinitely long pore the image forces contribute a term to the potential energy of a point charge located at a distance r from the interface

$$E_\varepsilon = \frac{\varepsilon_A - \varepsilon_L}{4\pi\varepsilon_A(\varepsilon_A+\varepsilon_L)} \cdot \frac{e}{r}. \tag{1}$$

ε_A, ε_L are the dielectric constants of the aqueous and lipid media, respectively. The contribution from the channel dipoles to the potential energy of a charge located on the axis of the cylindrical channel is calculated by assuming the dipoles to be uniformly smeared out over the channel wall. The result is

$$E_D = -\frac{p}{2\pi(\varepsilon_A+\varepsilon_L)\cdot R}\left(1-\frac{r}{\sqrt{r^2+R^2}}\right) \tag{2}$$

where p is the dipole moment per unit length of the channel and R is the radius of the channel. This term decreases monotonically as r goes from $+\infty$ (ouside the channel) to $-\infty$ (inside the channel) where the energy approaches a constant value.

Figure 1 shows an example ($\varepsilon_L \approx 0$, $p=\frac{1}{2}e$, $R=1$ Å) where the two energy terms are com-

[1] An alternative four-site model (3*B*4*S*′) where all the sites lie internal to the outer barriers has been considered elsewhere (Hägglund et al., 1982).

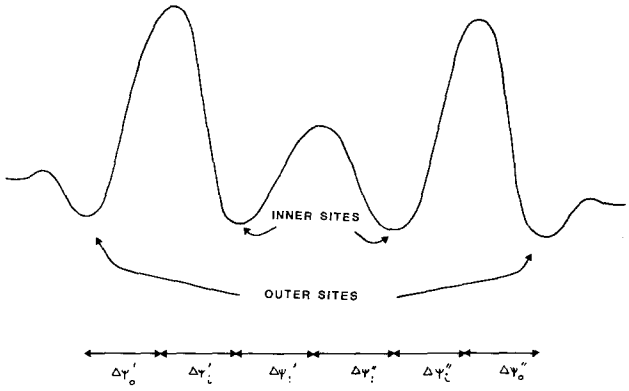

Fig. 2. Potential energy profile of the model, containing a pair of outer sites separated from the aqueous compartments by negligible barriers, and a pair of inner sites. The distribution of the total potential drop across the different peak-well steps are indicated with symbols explained in the text

bined to produce an energy minimum outside the channel. The size of the well corresponds to about $4kT$ and the distance away from the channel is about eight times the channel radius, which should be sufficient for the counter ions to screen the charge and diminish electrostatic interactions with ions in the channel interior.

Inside the channel the shape and location of the sites and barriers will depend on the polarizability of the channel wall and on specific ion-channel interactions. A discussion of the possible barrier profiles for the gramicidin A channel is found in the papers by Andersen (1982*a*, *b*), Eisenman et al. (1978), Finkelstein and Andersen (1981), Hägglund et al. (1981), and Urry et al. (1980), and in this treatment we will, in addition to the outer sites shown in Fig. 1, consider the interior to consist of three barriers and two sites.

The total energy profile of the channel thus assumed is shown in Fig. 2 with barriers at its middle and ends separating the inner and outer sites and where the latter are in equilibrium with the external solutions.

The theory developed for this system combines the treatment of multibarrier models by Heckmann (1965*a*, *b*; 1968) with the treatment of Sandblom et al. (1977) of a system with multiple equilibrium sites. By introducing energy levels of peaks and of wells it is shown that the equations describing the fluxes and electrical properties of the system can be written in forms which are easy to interpret.

First an outline of the general theory for two permeable ionic species will be given and the coefficients expressed in terms of energy levels of the peaks and of the wells for the different occupancy configurations. The explicit solution to the transport equations for a single permeable species will then be derived and used to study the properties of several important measurable quantities such as the conductance at zero current, the correlation factor and the current-voltage relationship.

General Theory

Description of the Channel

The energy profile for the $3B4S''$ channel is shown in Fig. 2 where the outermost barriers separating the outer sites from the aqueous solutions are considered to be small enough to produce a state of equilibrium between the outer sites and the aqueous solutions regardless of which of the three barriers is rate determining.

For simplicity, the positions of barriers and wells are assumed to be fixed in space, independent of ion occupancy, although it is possible to let the positions vary by letting the potential drops in Fig. 2 depend on the particular occupancy configurations (Urban & Hladky, 1979).

We use previous notations (Sandblom et al., 1977) and label outer and inner sites by o and i, respectively, and use a colon to indicate the central barrier. The superscripts $'$ and $''$ refer to the left and right channel halves, respectively, and to the left and right side bathing solutions.

We will, without any greater loss of generality, assume the applied electric field to lie entirely across the barriers in the channel, and the different potential steps which make up the total potential are labelled in Fig. 2. The potential is normalized with respect to RT/F and is labelled ψ.

Vectorial Representation

It is well known that a dynamic system which can make transitions between a finite number of discrete states can be represented by a state diagram (*cf.* Heckmann, 1965*a*, *b*; Chizmadjev & Aityan, 1977; Hille & Schwarz, 1978). Usually such a diagram describes each loading state explicitly where the molecular mechanism underlying the transitions between states (e.g., vacancy diffusion or correlated "knock-off" jumps) will determine how the lines, representing the various transition paths, will connect the different states. Even for a simple two-site mod-

el such a diagram is already quite complex when two different ionic species are present (having nine states). On extending the diagram to models with four sites the diagram becomes exceedingly cumbersome (with 81 states). However, by a vectorial representation of states and rate constants we can represent the present three-barrier four-site case by a diagram corresponding to the three-barrier two-site model.

We introduce vector quantities $\mathbf{N}$ and $\mathbf{v}$ to represent collections of state variables and rate constants, respectively. Each element N of a vector $\mathbf{N}$ represents a particular state variable and is distinguished by a subscript which indicates the occupancy configuration of the state. The symbol for the central peak (:) is added in the subscript to separate the two halves of the channel.

The symbol $N_{x_i:y_o}$, for example, represents the fraction of time during which the left inner site is occupied by an ion X, while at the same time the right outer site is occupied by an ion Y and the remaining sites are unoccupied.

By collecting all states containing a given occupancy configuration of the *inner* sites into a vector, we get the two-site state vector diagram shown in Fig. 3. In a system containing two-species, each such vector has nine components, for instance

$$\mathbf{N}_{oo}=\begin{bmatrix} N_{:} \\ N_{x_o:} \\ N_{y_o:} \\ N_{:x_o} \\ N_{:y_o} \\ N_{x_o:x_o} \\ N_{y_o:y_o} \\ N_{x_o:y_o} \\ N_{y_o:x_o} \end{bmatrix}, \quad \mathbf{N}_{ox}=\begin{bmatrix} N_{:x_i} \\ N_{x_o:x_i} \\ N_{y_o:x_i} \\ N_{:x_ix_o} \\ N_{:x_iy_o} \\ N_{x_o:x_ix_o} \\ N_{y_o:x_iy_o} \\ N_{x_o:x_iy_o} \\ N_{y_o:x_ix_o} \end{bmatrix}, \tag{3}$$

Since the vector is defined by two indices only, describing the occupancy configuration of the inner sites, it is convenient to indicate by zero an unoccupied inner site, and by x or y an occupied inner site, and there is no need for a colon in the subscripts of the vector symbols.

We will also make use of the quantity which is obtained by summing the elements of a state vector, the trace of the vector. We then get a lumped state variable which will be given the corresponding scalar notation. N_{oo}, and N_{ox}, for instance, are the lumped state variables corresponding to the vectors $\mathbf{N}_{oo}$ and $\mathbf{N}_{ox}$ and express the total probabilities for the indicated inner occupancies to occur.

Therefore, the total sum of lumped state variables taken over all possible inner occupancies must be equal to unity or

$$N_{oo}+N_{ox}+N_{xo}+\ldots=1. \tag{4}$$

Rate Vectors

The transitions between states which involve the passage of ions across one of the three barriers are characterized by rate constants. Each rate constant describes a transition between two states and hence, by collecting certain states into vectors, a corresponding collection of rate constants into vectors is automatically suggested. Since two elements of a particular state vector differ only with respect to their outer site occupancy we similarly define a rate vector as having elements which differ only with respect to their outer site occupancy configuration. With this definition we get vectors with varying number of elements, namely, three elements each for the outer barriers and nine elements for the inner barrier. This is seen from the examples given in Eq. (5) for two univalent cations where a subscript is assigned to each rate constant to indicate the starting condition of a transition and a superscript is added to indicate the final condition following the transition.

$$\begin{aligned} \mathbf{v}_{ox}^{oo}&=\exp(-\Delta\psi_i'')\begin{bmatrix} v_{:x_i}^{:x_o} \\ v_{x_o:x_i}^{x_o:x_o} \\ v_{y_o:x_i}^{y_o:x_o} \end{bmatrix}, \\ \mathbf{v}_{xo}^{ox}&=\exp(-\Delta\psi_i')\begin{bmatrix} v_{x_i:}^{:x_i} \\ v_{x_ox_i:}^{x_o:x_i} \\ v_{y_ox_i:}^{y_o:x_i} \\ v_{x_i:x_o}^{:x_ix_o} \\ v_{x_i:y_o}^{:x_iy_o} \\ v_{x_ox_i:x_o}^{x_o:x_ix_o} \\ v_{y_ox_i:y_o}^{y_o:x_iy_o} \\ v_{x_ox_i:y_o}^{x_o:x_iy_o} \\ v_{y_ox_i:x_o}^{y_o:x_ix_o} \end{bmatrix}, \ldots \end{aligned} \tag{5}$$

In order to clarify the symbols, the transitions corresponding to $\mathbf{v}_{ox}^{oo}$ in Eq. (5) are illustrated below with arrows.

$v_{:x_i}^{:x_o}$ 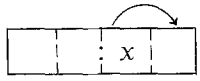

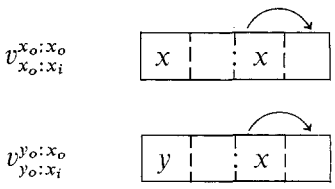

Each rate vector is associated with a particular barrier, a particular ion and a particular direction of jumping. The difference between the elements lies only in the outer site occupancy configurations, which is the reason why the outer barrier rate vectors have fewer elements than the inner barrier rate vectors. Since, however, the rate vectors will be used in vector operations we assign the same number of elements to all of them by letting certain rate constants be zero, namely, those describing a jump into an already occupied site (thereby excluding knock-off transitions).

Transition Rates

The rate of transition from one particular lumped state to another lumped state is given by the sum of all the individual transition rates where each individual transition rate is given by the product of the corresponding state variable and rate constant. The lumped transition rates are therefore given by the scalar products of the corresponding vectorial state variable and vectorial rate constant.

As an example, we take the total or lumped transition rate from state N_{ox} to N_{oo}, which can be written

$$-[\dot{N}_{ox}]_{N_{ox}\to N_{oo}} = \mathbf{N}_{ox}\cdot\mathbf{v}^{oo}_{ox}$$
$$= [N_{:x_i} v^{:x_o}_{:x_i} + N_{x_o:x_i} v^{x_o:x_o}_{x_o:x_i} + N_{y_o:x_i} v^{y_o:x_o}_{y_o:x_i}]$$
$$\cdot \exp(-\Delta\psi_i'') \tag{6}$$

and which contains all transitions from a right inner site X-occupancy to a right outer site X-occupancy when the left inner site is empty.

Similar equations can be written for all transitions in the state diagram of Fig. 3.

The usefulness of this formalism lies in the ability to transform the vector quantities into scalar lumped parameters, and this transformation is carried out with the use of equilibrium constants for binding to the channel sites.

Binding Constants

The binding constants are introduced by taking into account that the outer sites are in equilibrium with the aqueous solutions. This means that the exchange of ions between outer sites and aqueous solutions can be characterized completely by equilibrium binding constants.

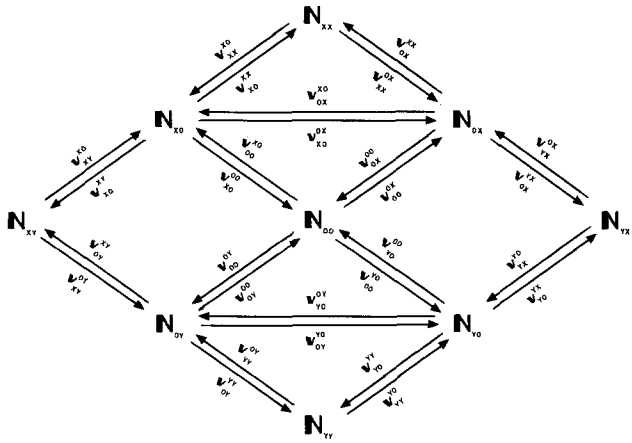

Fig. 3. Vector state diagram of the $3B4S''$ model where states and transition rate constants represent vectors

Two examples are given in Eq. (7) where S symbolizes the empty channel

$$X' + X_i'' S \rightleftharpoons X_o' X_i'' S \tag{7a}$$
$$X' + Y'' + X_i'' S \rightleftharpoons X_o' X_i'' Y_o'' S. \tag{7b}$$

Each of the reactions above defines a binding constant k which we write according to the law of mass action,

$$\frac{k_{x_o:x_i}}{k_{:x_i}} = \frac{N_{x_o:x_i}}{C_x' N_{:x_i}} \tag{8a}$$
$$\frac{k_{x_o:x_i y_o}}{k_{:x_i}} = \frac{N_{x_o:x_i y_o}}{C_x' C_y'' \cdot N_{:x_i}}. \tag{8b}$$

The reason for splitting each binding constant into a ratio of two constants is that we want to refer all binding constants to a common reference, the empty channel. If we therefore let $k_{:x_i}$ be the equilibrium binding constant for loading the right inner site of an empty channel with an ion of species X, then $k_{x_o:x_i}$ becomes the binding constant for loading both left outer and right inner sites with ions of species X, etc.

Rearranging Eq. (8) and adding all other binding constants corresponding to this particular right inner site occupancy gives

$$\frac{N_{:x_i}}{k_{:x_i}} = \frac{N_{x_o:x_i}}{C_x' k_{x_o:x_i}} = \frac{N_{x_o:x_i x_o}}{C_x' C_x'' k_{x_o:x_i x_o}} = \ldots = \frac{N_{ox}}{k_{ox}} \tag{9}$$

where

$$k_{ox} = k_{:x_i} + C'_x k_{x_o:x_i} + C''_x k_{:x_i x_o} + C'_y k_{y_o:x_i} + C''_y k_{:x_i y_o} + C'_x C''_x k_{x_o:x_i x_o} + C'_y C''_y k_{y_o:x_i y_o} + C'_x C''_y k_{x_o:x_i y_o} + C'_y C''_x k_{y_o:x_i x_o}. \quad (10)$$

k_{ox} is a lumped parameter which we call a *well function* to emphasize that it is independent of the barrier heights.

If we regard each denominator in Eq. (9) as an element of a binding vector, e.g., $\mathbf{k}_{ox} = (k_{:x_i}, C'_x k_{x_o:x_i}, C''_x C'_x k_{x_o:x_i x_o}, \ldots)$ we can rewrite Eq. (9) as

$$\mathbf{N}_{ox} = \mathbf{k}_{ox} \cdot \frac{N_{ox}}{k_{ox}} \quad (11)$$

and if we insert this in Eq. (6) we get

$$-[\dot{N}_{ox}]_{N_{ox} \to N_{oo}} = \mathbf{N}_{ox} \cdot \mathbf{v}^{xx}_{ox} = N_{ox} \frac{\mathbf{k}_{ox} \cdot \mathbf{v}^{oo}_{ox}}{k_{ox}}. \quad (12)$$

In this way we can express the entire set of rate equations in terms of lumped state variables and rate constants which consist of scalar products between binding and rate vectors divided by the well functions.

Lumped Rate Constants

Eq. (12) defines a quantity which we label v^{oo}_{ox}

$$v^{oo}_{ox} = \frac{\mathbf{k}_{ox} \cdot \mathbf{v}^{oo}_{ox}}{k_{ox}} = \frac{[k_{:x_i} v^{:x_o}_{:x_i} + C'_x k_{x_o:x_i} v^{x_o:x_o}_{x_o:x_i} + C'_y k_{y_o:x_i} v^{y_o:x_o}_{y_o:x_i}] \exp(-\Delta\psi''_i)}{k_{ox}} \quad (13)$$

and which is seen to be proportional to the sum of the individual rate constants multiplied by coefficients containing the binding constants. Since each such coefficient is proportional to the equilibrium occupancy of the corresponding state we can view Eq. (13) as defining an average or *lumped rate constant* v^{oo}_{ox}. A lumped rate constant is therefore the weighted sum of the vector elements where the weighting factors are the corresponding equilibrium occupancies of the outer sites.

This lumping procedure will condense the rate equations for the $3B4S''$ system into a set of equations corresponding to a $3B2S$ model. It also incorporates all types of binding to the outer sites, for instance ion pairs (anions + cations) or blocking ions like divalent ions, etc. This will appear as additional terms in the **k** and **v** vectors but will not alter the basic two-site state diagram of Fig. 3 nor the rate equations derived from it.

Peak Functions

In order to incorporate the equations of detailed balance for the lumped rate constants it is convenient to define another function, a *peak function p*, which we define from Eq. (13) as follows

$$v^{oo}_{ox} = \frac{\exp(-\Delta\psi''_i) p^{oo}_{ox}}{k_{ox}}$$

where

$$p^{oo}_{ox} = k_{:x_i} v^{:x_o}_{:x_i} + C'_x k_{x_o:x_i} v^{x_o:x_o}_{x_o:x_i} + C'_y k_{y_o:x_i} v^{y_o:x_o}_{y_o:x_i}. \quad (14)$$

Each term in the expression for p^{oo}_{ox}, Eq. (14), contains a product between a binding constant and a rate constant and therefore defines a peak (energy of an activated state). Since the energy level of a particular state (whether equilibrium or activated state) is independent of the pathway by which it is reached, we can derive a series of relationships between the different p-parameters (peak functions).

For p^{oo}_{ox}, we get

$$\begin{aligned} p^{oo}_{ox} &= k_{:x_i} v^{:x_o}_{:x_i} + C'_x k_{x_o:x_i} v^{x_o:x_o}_{x_o:x_i} + C'_y k_{y_o:x_i} v^{y_o:x_o}_{y_o:x_i} \\ &= k_{:x_o} v^{:x_i}_{:x_o} + C'_x k_{x_o:x_o} v^{x_o:x_i}_{x_o:x_o} + C'_y k_{y_o:x_o} v^{y_o:x_i}_{y_o:x_o} \\ &= p^{ox}_{oo}. \end{aligned} \quad (15)$$

Similar relationships are derived for all other peak functions and from which we draw the general conclusion that the super and subscripts in the peak parameters as well as in the peak functions can be interchanged without altering their identities.

Such relationships also lead to equations of detailed balance for the lumped parameter system. As an example, we get for the upper loop in Fig. 3, in the absence of chemical and electrical potential differences,

$$\begin{aligned} v^{xo}_{oo} v^{ox}_{xo} v^{oo}_{ox} &= C_x \frac{p^{xo}_{oo} p^{ox}_{xo} p^{oo}_{ox}}{k_{oo} k_{xo} k_{ox}} \\ &= C_x \frac{p^{oo}_{xo} p^{xo}_{ox} p^{ox}_{oo}}{k_{xo} k_{ox} k_{oo}} = v^{oo}_{xo} v^{xo}_{ox} v^{ox}_{oo}. \end{aligned} \quad (16)$$

Since the products between rate constants and binding constants in Eq. (15) constitute peak terms which are independent of the jump direc-

Table 1.

	Rate constant	Well function	Peak function
υ_{ox}^{xo}	$\exp(\Delta\psi_{:}'')\frac{p_{ox}^{xo}}{k_{ox}}$		$\left.\begin{matrix}p_{ox}^{xo}\\ p_{xo}^{ox}\end{matrix}\right\}=\begin{matrix}p_{\bar{x}}+C_x'p_{x_o\bar{x}}\\ +C_x''p_{\bar{x}x_o}+C_x'C_x''p_{x_o\bar{x}x_o}\end{matrix}$
υ_{xo}^{ox}	$\exp(-\Delta\psi_{:}')\frac{p_{xo}^{ox}}{k_{xo}}$	$k_{xo}=k_{x_i:}+C_x'k_{x_ox_i:}+C_x''k_{x_i:x_o}+C_x'C_x''k_{x_ox_i:x_o}$	
υ_{oo}^{ox}	$C_x''\exp(\Delta\psi_{o}'')\frac{p_{oo}^{ox}}{k_{oo}}$		$\left.\begin{matrix}p_{oo}^{ox}\\ p_{ox}^{oo}\end{matrix}\right\}=p_{:\bar{x}}+C_x'p_{x_o:\bar{x}}$
υ_{ox}^{oo}	$\exp(-\Delta\psi_{i}')\frac{p_{ox}^{oo}}{k_{ox}}$	$k_{ox}=k_{:x_i}+C_x'k_{x_o:x_i}+C_x''k_{:x_ix_o}+C_x'C_x''k_{x_o:x_ix_o}$	
υ_{oo}^{xo}	$C_x'\exp(-\Delta\psi_{o}')\frac{p_{oo}^{xo}}{k_{oo}}$		$\left.\begin{matrix}p_{oo}^{xo}\\ p_{xo}^{oo}\end{matrix}\right\}=p_{\bar{x}:}+C_x''p_{\bar{x}:x_o}$
υ_{xo}^{oo}	$\exp(\Delta\psi_{i})\frac{p_{xo}^{oo}}{k_{xo}}$	$k_{oo}=1+C_x'k_{x_o:}+C_x''k_{:x_o}+C_x'C_x''k_{x_o:x_o}$	
υ_{xo}^{xx}	$C_x''\exp(\Delta\psi_{o}'')\frac{p_{xo}^{xx}}{k_{xo}}$		$\left.\begin{matrix}p_{xx}^{xo}\\ p_{xx}^{xx}\end{matrix}\right\}=p_{x_i:\bar{x}}+C_x'p_{x_ox_i:\bar{x}}$
υ_{xx}^{xo}	$\exp(-\Delta\psi_{i}')\frac{p_{xx}^{xo}}{k_{xx}}$	$k_{xx}=k_{x_i:x_i}+C_x'k_{x_ox_i:x_i}+C_x''k_{x_i:x_ix_o}+C_x'C_x''k_{x_ox_i:x_ix_o}$	
υ_{ox}^{xx}	$C_x'\exp(-\Delta\psi_{o}')\frac{p_{ox}^{xx}}{k_{ox}}$		$\left.\begin{matrix}p_{xx}^{ox}\\ p_{ox}^{xx}\end{matrix}\right\}=p_{\bar{x}:x_i}+C_x''p_{\bar{x}:x_ix_o}$
υ_{xx}^{ox}	$\exp(\Delta\psi_{i}')\frac{p_{xx}^{ox}}{k_{xx}}$		

tions, it is appropriate to label the peak terms with the single letter p. The subscript attached to this symbol describes the location of ions in the activated state analogous to the subscript of the binding constants. If we indicate by $\bar{X}$ an ion of species X on top of a barrier we can rewrite Eq. (15) in terms of peaks as follows

$$\left.\begin{matrix}p_{ox}^{oo}\\ p_{oo}^{xo}\end{matrix}\right\}=p_{:\bar{x}}+C_x'p_{x_o:\bar{x}}+C_y'p_{y_o:\bar{x}}. \tag{17}$$

Table 1 summarizes the relationships between lumped and intrinsic parameters for the $3B4S''$ system with a single species X.

Since the equations for the transition rates (Eq. 12), which contain the equations of detailed balance when written in terms of lumped parameters (Eq. 14), are identical to those of a two-site system, we can solve the transport equations for the $3B2S$-model and then express the lumped parameters in terms of the intrinsic parameters from equations shown in Table 1. We will follow this procedure in the following sections in order to develop of formalism useful for experimental purposes.

Results

Solutions to the Transport Equations for a Single Permeable Species at Steady State

The net steady-state flow of a species (X) through the channel is given by the sum of all possible transitions across any one of the barriers, and if we choose the middle barrier we can write the total flow across it as

$$J_x=\boldsymbol{v}_{xo}^{ox}\cdot\boldsymbol{N}_{xo}-\boldsymbol{v}_{ox}^{xo}\cdot\boldsymbol{N}_{ox}=\upsilon_{xo}^{ox}N_{xo}-\upsilon_{ox}^{xo}N_{ox}. \tag{18}$$

The lumped state variables N_{xo} and N_{ox} are solved in terms of the lumped rate constants from the equations of mass balance for each state.

$$\dot{N}_{xx}=0=\upsilon_{ox}^{xx}N_{ox}+\upsilon_{xo}^{xx}N_{xo}-(\upsilon_{xx}^{ox}+\upsilon_{xx}^{xo})N_{xx} \tag{19a}$$

$$\dot{N}_{oo}=0=\upsilon_{ox}^{oo}N_{ox}+\upsilon_{ox}^{oo}N_{xo}-(\upsilon_{oo}^{ox}+\upsilon_{oo}^{xo})N_{oo} \tag{19b}$$

$$\dot{N}_{ox}=0=\upsilon_{xx}^{ox}N_{xx}+\upsilon_{oo}^{ox}N_{oo}+\upsilon_{xo}^{ox}N_{xo}-(\upsilon_{ox}^{oo}+\upsilon_{ox}^{xx}+\upsilon_{ox}^{xo})N_{ox} \tag{19c}$$

$$\dot{N}_{xo}=0=v_{xx}^{xo}N_{xx}+v_{oo}^{xo}N_{oo}+v_{ox}^{xo}N_{ox}-(v_{xo}^{oo}+v_{xo}^{xx}+v_{xo}^{ox})N_{xo}. \quad (19d)$$

Three of these equations, in combination with Eq. (1) which for a single species reduces to

$$N_{oo}+N_{ox}+N_{xo}+N_{xx}=1 \quad (20)$$

are sufficient to obtain solutions for the state variables. The two-state variables N_{ox} and N_{xo} are solved from Eqs. (19) and (20) and inserted in Eq. (18) which gives

$$J_x=\frac{v_{xo}^{ox}(V_{ox}^{oo}+V_{ox}^{xx})-v_{ox}^{xo}(V_{xo}^{oo}+V_{xo}^{xx})}{(v_{xo}^{ox}+V_{xo}^{oo}+V_{xo}^{xx})\left(1+\frac{V_{ox}^{oo}}{v_{oo}^{xo}}+\frac{V_{ox}^{xx}}{v_{xx}^{xo}}\right)+(v_{ox}^{xo}+V_{ox}^{oo}+V_{ox}^{xx})\left(1+\frac{V_{xo}^{oo}}{v_{oo}^{ox}}+\frac{V_{xo}^{xx}}{v_{xx}^{ox}}\right)} \quad (21)$$

where the following abbreviating symbols have been used

$$V_{ox}^{oo}=\frac{v_{ox}^{oo}v_{oo}^{xo}}{v_{oo}^{ox}+v_{oo}^{xo}},\quad V_{xo}^{oo}=\frac{v_{xo}^{oo}v_{oo}^{ox}}{v_{oo}^{ox}+v_{oo}^{xo}}$$

$$V_{ox}^{xx}=\frac{v_{ox}^{xx}v_{xx}^{xo}}{v_{xx}^{ox}+v_{xx}^{xo}},\quad V_{xo}^{xx}=\frac{v_{xo}^{xx}v_{xx}^{ox}}{v_{xx}^{ox}+v_{xx}^{xo}}. \quad (22)$$

An equation similar to Eq. (21) has been derived by Urban and Hladky (1979) and the difference lies in the explicit concentration dependence of the rate constants (given in Table 1).

In order to introduce this concentration dependence, using Table 1, the expressions for the lumped rate constants (Table 1) are first inserted in Eq. (22)

$$V_{ox}^{oo}=\frac{C_x'\exp(-\Delta\psi_{oi}')}{k_{ox}}\cdot P_x \quad (23a)$$

$$V_{xo}^{oo}=\frac{C_x''\exp(\Delta\psi_{oi}'')}{k_{xo}}\cdot P_x \quad (23b)$$

$$V_{ox}^{xx}=\frac{C_x'\exp(-\Delta\psi_{oi}')}{k_{ox}}\cdot P_{xx} \quad (23c)$$

$$V_{xo}^{xx}=\frac{C_x''\exp(\Delta\psi_{oi}'')}{k_{xo}}\cdot P_{xx} \quad (23d)$$

where P_x and P_{xx} are defined as

$$P_x=\left[\frac{C_x'\exp(-\Delta\psi_{oi}')}{p_{ox}^{oo}\exp(-\Delta\psi_i'')}+\frac{C_x''\exp(\Delta\psi_{oi}'')}{p_{xo}^{oo}\exp(\Delta\psi_i')}\right]^{-1} \quad (24a)$$

$$P_{xx}=\left[\frac{1}{p_{xx}^{xo}\exp(-\Delta\psi_i'')}+\frac{1}{p_{xx}^{ox}\exp(\Delta\psi_i')}\right]^{-1} \quad (24b)$$

and where $\Delta\psi_{oi}'=\Delta\psi_o'+\Delta\psi_i'$, $\Delta\psi_{oi}''=\Delta\psi_o''+\Delta\psi_i''$ are the potential differences between the outer and inner sites.

When Eq. (23) and the expressions for v_{ox}^{xo}, v_{xo}^{ox} obtained from Table 1 are substituted in Eq. (21) we get after rearrangement

$$J_x=(C_x'\exp(-\Delta\psi')-C_x''\exp(\Delta\psi''))\cdot\left[\frac{1}{N_s^{1B4S}\cdot p_{xo}^{ox}}+\frac{\exp(-\Delta\psi_i'+\Delta\psi_i'')}{N_s^{2B4S}(P_x+P_{xx})\sqrt{C_x'C_x''\exp(-\Delta\psi'+\Delta\psi'')}}\right]^{-1} \quad (25)$$

where $\Delta\psi'$, $\Delta\psi''$ are the total potential differences across each half of the channel and where [2]

$$1/N_s^{1B4S}=k_{oo}+k_{xo}C_x'\exp(-\Delta\psi_{oi}')+k_{ox}C_x''\cdot\exp(\Delta\psi_{oi}'')+k_{xx}C_x'C_x''\exp(-\Delta\psi_{oi}'+\Delta\psi_{oi}'') \quad (26a)$$

$$1/N_s^{2B4S}=k_{oo}P_x\left[\frac{C_x'\exp(-\Delta\psi_{oi}'+\Delta\bar{\mu}/2)}{p_{ox}^{oo}\exp(-\Delta\psi_i'')}+\frac{C_x''\exp(\Delta\psi_{oi}''-\Delta\bar{\mu}/2)}{p_{xo}^{oo}\exp(\Delta\psi_i')}\right]+k_{xo}C_x''\cdot\exp(-\Delta\psi_{oi}'+\Delta\bar{\mu}/2)+k_{ox}C_x''\exp(\Delta\psi_{oi}''-\Delta\bar{\mu}/2)+k_{xx}P_{xx}C_x'C_x''\exp(-\Delta\psi_{oi}'+\Delta\psi_{oi}'')\cdot\left[\frac{\exp(-\Delta\bar{\mu}/2)}{p_{xx}^{xo}\exp(-\Delta\psi_i'')}+\frac{\exp(\Delta\bar{\mu}/2)}{p_{xx}^{ox}\exp(\Delta\psi_i')}\right] \quad (26b)$$

$\Delta\bar{\mu}$ is the electrochemical potential difference across the membrane, i.e.

$$\Delta\bar{\mu}=-\ln\frac{C_x'}{C_x''}+(\Delta\psi'+\Delta\psi''). \quad (27)$$

The bracketed term in Eq. (25) is seen to consist of two terms which separate the outer and middle barriers with respect to peak parameters. The first term contains only the peak parameters of the middle barrier whereas the second term contains only the peak parameters of the outer barriers. This means that the first term dominates over the second if the middle barrier is rate limiting ($p_{xo}^{ox}\ll P_x, P_{xx}$), and the expression reduces to that of a 1-barrier four-site system (1*B*4*S*)

[2] The subscript *s* in N_s^{1B4S}, N_s^{2B4S} symbolizes the empty channel and is added to indicate that at equilibrium the quantities N_s^{1B4S}, N_s^{2B4S} become equal to the probability that the channel is empty (zero occupancy, *see* below). The reason for the superscripts 1*B*4*S* and 2*B*4*S* are given below.

$$J_x = N_s^{1B4S} p_{xo}^{ox}(C'_x \exp(-\Delta\psi') - C''_x \exp(\Delta\psi'')) \quad (1B4S \text{ limit}). \tag{28a}$$

The properties of this equation has been described in detail by Sandblom et al. (1977).

If, on the other hand, the middle barrier is very small ($p_{xo}^{ox} \gg P_x$, P_{xx}) so that the outer barriers are rate limiting the expression reduces to that of a two-barrier four-site system ($2B4S$)

$$J_x = N_s^{2B4S}(P_x + P_{xx}) \exp(\Delta\psi'_{:} - \Delta\psi''_{:}) \cdot \sqrt{C'_x C''_x \exp(-\Delta\psi' + \Delta\psi'')}\,[C'_x \exp(-\Delta\psi') - C''_x \exp(\Delta\psi'')] \quad (2B4S \text{ limit}) \tag{28b}$$

and is a case which can be fitted reasonably well to experimental data for CsCl in gramicidin A channels as will be shown below.

The net flux through the membrane can therefore be written in the form

$$\frac{1}{J_x^{3B4S}} = \frac{1}{J_x^{1B4S}} + \frac{1}{J_x^{2B4S}} \tag{29}$$

and which is a convenient way to describe the contributions from the different rate limiting steps, the central barrier ($1B4S$ model) and the outer barriers ($2B4S$ model).

At equilibrium ($\Delta\bar{\mu} = 0$) the expression for N_s^{2B4S} is seen by taking into account be expressions for P_x, P_{xx} Eqs. (24), to reduce to that for N_s^{1B4S}, i.e.

$$\begin{aligned} 1/N_s^{2B4S} &= 1/N_s^{1B4S} = 1/N_s \\ &= 1 + C'_x[k_{y_o:} + k_{x_i:} \exp(-\Delta\psi'_{oi})] \\ &\cdot C''_x[k_{:x_o} + k_{:x_i} - \exp(\Delta\psi''_{oi})] + C'^2_x k_{x_o x_i:} \\ &\cdot \exp(-\Delta\psi'_{oi}) + C''^2_x k_{:x_i x_o} \exp(\Delta\psi''_{oi}) \\ &+ C'_x C''_x[k_{x_o:x_o} + k_{x_o:x_i} \exp(\Delta\psi''_{oi}) + k_{x_i:x_o} \\ &\cdot \exp(-\Delta\psi'_{oi}) + k_{x_i:x_i} \exp(-\Delta\psi'_{oi} + \Delta\psi''_{oi})] \\ &+ C'^2_x C''_x[k_{x_o x_i:x_o} \exp(-\Delta\psi'_{oi}) + k_{x_o x_i:x_i} \\ &\cdot \exp(-\Delta\psi'_{oi} + \Delta\psi''_{oi})] + C'_x C''^2_x[k_{x_o:x_i x_o} \exp(\Delta\psi''_{oi}) \\ &+ k_{x_i:x_i x_o} \exp(-\Delta\psi'_{oi} + \Delta\psi''_{oi})] + C'^2_x C''^2_x k_{x_o x_i:x_i x_o} \\ &\cdot \exp(-\Delta\psi'_{oi} + \Delta\psi''_{oi}) \end{aligned} \tag{30}$$

where the lumped parameters have been expanded in the individual binding constants according to Table 1.

In the following we will consider a few special cases of Eqs. (25), (26) and (30) confined to symmetrical channels with equal concentrations on both sides of the membrane.

Equilibrium occupancy

Rewriting Eq. (30) for a symmetrical channel with

$$1/N_s = 1 + 2K_1 C_x + K_2 C_x^2 + 2K_3 C_x^3 + K_4 C_x^4 \tag{31}$$

where

$$K_1 = k_{x_o} + k_{x_i} \tag{32a}$$

$$K_2 = k_{x_o x_o} + 2k_{x_o x_i} + k_{x_i x_i} \tag{32b}$$

$$K_3 = k_{x_o x_i x_o} + k_{x_o x_i x_i} \tag{32c}$$

$$K_4 = k_{x_o x_i x_i x_o}. \tag{32d}$$

In view of the symmetry, a colon in the subscript is not needed and we have also put $k_{x_o x_i:} + k_{x_i:x_o} = k_{x_o x_i}$.

The K-parameters appearing in Eq. (31) are seen to contain successively the binding constants for binding one, two, three and four ions and are therefore directly proportional to the occupancy, i.e., the probability that a particular number of ions occupy the channel. The probabilities for the different occupancies can therefore be written

$$\frac{P(0)}{1} = \frac{P(1)}{2K_1 C_x} = \frac{P(2)}{K_2 C_x^2} = \frac{P(3)}{2K_3 C_x^3} = \frac{P(4)}{K_4 C_x^4} \tag{33}$$

and from the condition that the sum of the probabilities must be equal to unity, we get

$$P(0) = (1 + 2K_1 C_x + K_2 C_x^2 + 2K_3 C_x^3 + K_4 C_x^4)^{-1} = N_s \tag{34a}$$

$$P(1) = 2K_1 C_x N_s \tag{34b}$$

$$P(2) = K_2 C_x^2 N_s \tag{34c}$$

$$P(3) = 2K_3 C_x^3 N_s \tag{34d}$$

$$P(4) = K_4 C_x^4 N_s. \tag{34e}$$

It is useful, in characterizing the channel properties, to correlate the concentration dependence of different measured parameters such as conductance, flux ratio exponent, etc., with the occupancy level (Hille & Schwartz, 1978; Hägglund et al., 1982), and we will use this below in describing the behavior of gramicidin A channels.

Conductance at Zero Current

The zero current conductance is defined as

$$G_x^0 = \left(\frac{J_x}{\Delta\psi}\right)_{\Delta\psi \to 0} \tag{35}$$

and is obtained from Eq. (25) by setting $\Delta\psi = 0$. For a symmetrical channel with equal concentrations on both sides, the zero current conductance reduces to

$$G_x^0 = N_s C_x \left[\frac{1}{p_{xo}^{ox}} + \frac{1}{(P_x + P_{xx})C_x}\right]^{-1}$$
$$= N_s C_x \left[\frac{1}{p_{xo}^{ox}} + \frac{1}{\left[\frac{C_x}{p_{ox}^{oo}} + \frac{C_x}{p_{xo}^{oo}}\right]^{-1} C_x + \left[\frac{1}{p_{xx}^{xo}} + \frac{1}{p_{xx}^{ox}}\right]^{-1} C_x}\right]^{-1} \quad (36)$$

where the limiting values of P_x and P_{xx} (Eqs. 24) at zero potential have been used and where N_s, the zero occupancy probability, is given by Eq. (31). By expanding the p-parameters according the Table 1 and by lumping the coefficients of the concentration terms as follows

$$\begin{aligned} P_1' &= p_{\bar{x}} & P_1'' &= p_{\bar{x}:} \\ P_2' &= p_{x_o\bar{x}} & P_2'' &= p_{\bar{x}:x_o} + p_{\bar{x}:x_i} \\ P_3' &= p_{x_o\bar{x}x_o} & P_3'' &= p_{\bar{x}:x_ix_o} \end{aligned} \quad (37a)$$

we can rewrite Eq. (36)

$$G_x^0 = N_s C_x \left[\frac{1}{P_1' + 2P_2' C_x + P_3' C_x^2} + \frac{2}{P_1'' + P_2'' C_x + P_3'' C_x^2}\right]^{-1}. \quad (37b)$$

From Eq. (37b) it is seen that both of the polynomials containing the P-parameters have the same degree with respect to the concentration terms, which means that the peak functions for the outer and middle barriers have the same concentration dependence.

In the $3B2S$ limit (when $p_{x_o\bar{x}} = p_{x_o\bar{x}x_o} = p_{\bar{x}:x_o} = p_{\bar{x}:x_ix_o} = 0$), Eq. (37b) reduces to

$$G_x^0 = N_s C_x \left(\frac{1}{P_1'} + \frac{1}{P_1'' + P_2'' C_x}\right)^{-1} \quad (38)$$

and at high concentrations the second term becomes negligible, which means that the middle barrier is rate determining. This high concentration limit behavior is one of the important features distinguishing models with outer saturable sites facing the aqueous solutions from those where ions jump directly from the aqueous solutions across barriers into the channel.

Since the high and low concentration behavior of the channel is useful both for distinguishing between different models and for fixing certain parameters it is necessary to set criteria for when the concentrations are high or low. We do this by means of the occupancies and define the low concentration end as the region where the channel is primarily empty and the current is carried by a single ion occupying the channel.

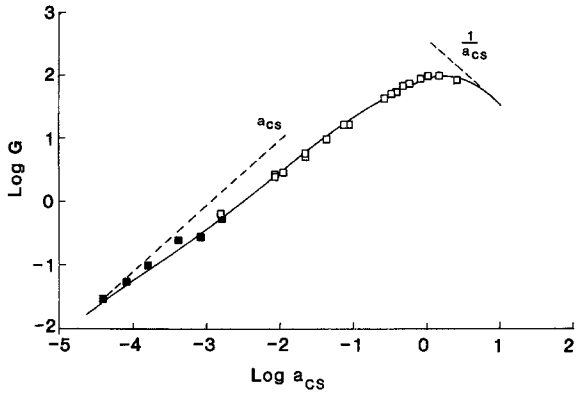

Fig. 4. The logarithm of the conductance is plotted against the logarithm of activity to define the high and low concentration ends. At low concentrations the conductance varies linearly with the ionic activity and at high concentrations the conductance varies inversely with the ionic activity. The regions of limiting behavior are indicated by the dotted lines

The high concentration end is defined similarly as the region where the channel is fully occupied and where the current is "carried" by a single vacancy (a single vacant site).

These regions can be determined experimentally from G^0 measurements by noting that when a single ion carries the current and the channel is primarly empty the conductance varies proportionally to the concentration, regardless of the model. When the channel is mostly fully occupied and a single vacancy carries the current the conductance varies inversely to the concentration for all models having two or more sites.

Figure 4 shows the behavior of G_x^0 for CsCl in gramicidin A channels where the indicated high and low concentration regions are defined by the straight lines.

The open squares in Fig. 4 represent data for Cs single channel conductance (Neher, Sandblom & Eisenman, 1978), and the filled squares are noise data (E. Neher, G. Eisenman and J. Sandblom, *unpublished*). The solid curve is a fit to the data of the $2B4S''$ model, Eq. (37b) with P_1', P_2' and $P_3' \approx \infty$. The dashed lines show the regions of low and high concentrations, respectively, and it is seen that, whereas the noise data covers a large range of the low concentration end, the single channel conductance data only extend to (and include) the transition regions at the high and low concentration ends.

Equivalent Circuit Representation

It is useful for describing the behavior of G_x^0 and for comparison with other models to repre-

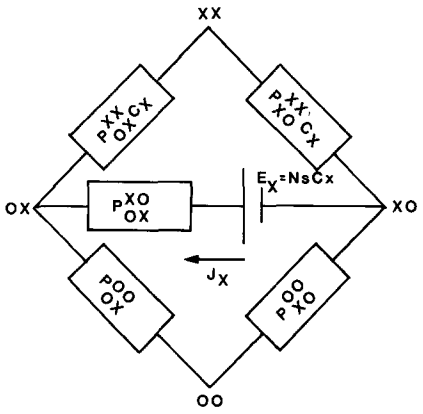

Fig. 5. Equivalent circuit of G_x^o consisting of a resistive network connected to a battery with the indicated emf. N_s is given by Eq. (34), and the conductance of each element is shown in the respective box

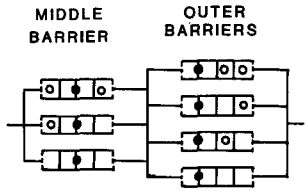

Fig. 6. Equivalent circuit of G_x^o derived from that in Fig. 5 by omitting the battery and expanding the resistive elements into parallel elements, each representing an activated state. The corresponding state is given by the configuration in the element, where a circle in a box represents an occupied site and where a filled circle on a line represents an ion at a peak. The solid lines dividing the boxes represent rate-limiting barriers and the dotted lines represent nonrate-limiting barriers

sent the peak part of Eq. (36), i.e., $G_x^0/N_s C_x$, in the form of an equivalent circuit.

If we view the bracketed term in Eq. (36) as a resistance it is clear that it is composed of two serial components, the first representing the middle barrier and the second representing the outer barriers. The second part can be further split into two branches so that the entire equation is represented by the circuit shown in Fig. 5.

The conductance of each element is indicated in the respective block and is seen to depend on the corresponding peak functions. Since, however, the peak functions themselves consist of sums of elements (Table 1) they can be represented by a parallel series of conductive elements, and if we therefore represent each peak parameter by a conductor (resistor), the circuit corresponding to Eq. (36) will appear as in Fig. 6 where the left part of the circuit represents the middle barrier and the right part the outer barriers and where the battery has been omitted.

Furthermore, since a peak parameter corresponds to a particular activated state we have used the resistive blocks to indicate the geometrical configuration of the corresponding activated state, where each box represents a well (site) and each vertical line represents a barrier. An unfilled circle in a box represents an occupied site and a filled circle on a line represents an occupied peak. The dotted lines indicate non rate-limiting barriers, i.e., where transitions occur rapidly compared to those taking place across the rate-limiting barriers (solid lines).

We can now draw several conclusions directly from Fig. 6 by noting that each peak parameter is multiplied by a concentration term (*see* Table 1), the power of which is equal to the corresponding occupancy of the sites, i.e., the number of unfilled circles within a block. The conductance of blocks containing unfilled circles are therefore concentration dependent, approaching zero at low concentrations and infinity at high concentrations.

It is seen that, if we omit all blocks with outer sites (thereby reducing the circuit to that of the 3*B*2*S* model), we are left with a single concentration independent conductance representing the middle barrier. The outer barriers, on the other hand, will have one concentration independent conductor which is short circuited at high concentrations, leaving the middle barrier resistor as the rate-limiting element.

For the complete 3*B*4*S*″ model, however, the circuit in Fig. 6 shows that both outer and middle barrier conductors at the top contain two unfilled circles and will not differ with respect to their concentration dependence at high concentrations.

Figure 7 shows the equivalent circuit representation of a few models that have been described in the literature. All of them have the same expression for N_s except the 3*B*2*S* model for which all terms containing x_o will vanish in Eq. (32). From this it is seen that the 3*B*4*S*′ model which has all sites internal to the outer barriers (Hägglund et al., 1982) shares the property with the 3*B*2*S* model that the middle barrier becomes rate limiting at high concentrations due to the fact that the maximum oc-

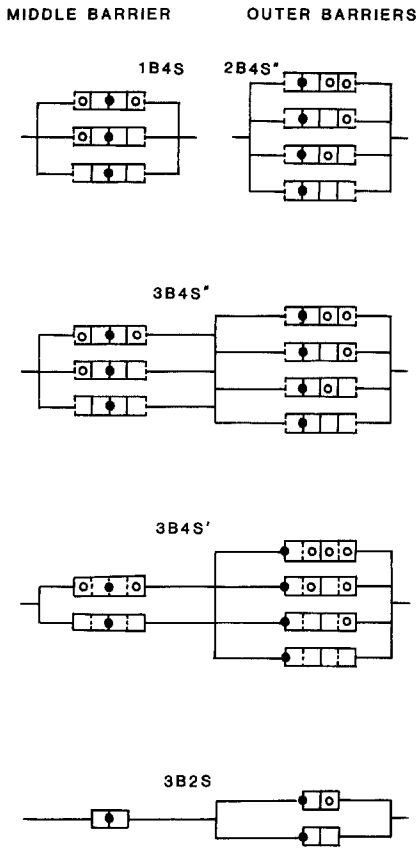

Fig. 7. Equivalent circuit representations of a few single filing models described in the literature

cupancy number of the middle barrier element is lower than that for the outer barriers (*see* Fig. 7).

This high concentration limit behavior which distinguishes models having outer sites in equilibrium with the aqueous solutions from other models will also affect other important measurable parameters, as will be seen in the following sections.

Apart from being a descriptive representation of the conductance behavior, the equivalent circuit representation is also a useful method for deriving the transport equations from the state diagram and will be used below in deriving an expression for the correlation factor. A more general network theory for converting state diagrams into equivalent circuits has been presented elsewhere (Sandblom, Ring & Eisenman, 1982).

Current Voltage Relationship

The current-voltage relationship for the general case is given in Eq. (25). For the special case of a symmetrical channel with equal concentrations on both sides, this equation can be reduced and written as

$$J_x = 2\sinh\left(-\frac{\Delta\psi}{2}\right) C_x \left[(p_{xo}^{ox})^{-1}(k_{oo}+k_{ox}C_x \cdot 2\cosh\Delta\psi_{oi}+k_{xx}C_x^2)+2\left(\frac{p_{ox}^{oo}}{\cosh\Delta\psi_o}+\frac{C_x p_{xx}^{ox}}{\cosh\Delta\psi_i}\right)^{-1} \cdot\left(k_{oo}\frac{\cosh(\Delta\psi_i+\Delta\psi_:)}{\cosh\Delta\psi_o}+2k_{ox}C_x\cosh\Delta\psi_: +k_{xx}C_x^2\frac{\cosh(\Delta\psi_o+\Delta\psi_:)}{\cosh\Delta\psi_i}\right)\right]^{-1} \quad (39)$$

where $\Delta\psi$ is the total membrane potential and where

$$\begin{aligned} k_{oo} &= 1+2k_{x_o}C_x+k_{x_ox_o}C_x^2 \\ k_{ox} &= k_{xo}=k_{x_i}+k_{x_ox_i}C_x+k_{x_ox_ix_o}C_x^2 \\ k_{xx} &= k_{x_ix_i}+2k_{x_ix_ix_o}C_x+k_{x_ox_ix_ix_o}C_x^2 \end{aligned} \quad (40a)$$

$$\begin{aligned} p_{ox}^{xo} &= p_{xo}^{ox}=p_{\bar{x}}+2p_{\bar{x}x_o}C_x+p_{x_o\bar{x}x_o}C_x^2 \\ p_{ox}^{oo} &= p_{xo}^{oo}=p_{\bar{x}:}+p_{\bar{x}:x_o}C_x \\ p_{xx}^{ox} &= p_{xx}^{xo}=p_{x_i:\bar{x}}+p_{x_ox_i:\bar{x}}C_x. \end{aligned} \quad (40b)$$

It is evident that each of the parameters is associated with a particular voltage and concentration dependent factor and that by measuring the current for an entire set of voltage and concentration values it is in principle possible to extract all the energy parameters of the system.

Although the number of independent parameters is large, the uniqueness of a model can usually be established by examining the behavior in certain limits. The shape of the *I–V* curve at low concentrations, for instance, is a property which allows the shape and size of the barriers to be determined rather accurately for the empty channel (Eisenman et al., 1980, 1982; Andersen, 1982*a*, *b*) and this information can then be used to fix a number of parameters in attempts to fit the entire model to experimental data.

At *high concentrations* the shape will also serve to distinguish between different models. The high concentration limit of Eq. (39) is given by

$$J_x = \frac{2\sinh\left(-\frac{\Delta\psi}{2}\right)}{k_{x_ox_ix_ix_o}C_x}[(p_{x_o\bar{x}x_o})^{-1}+2(p_{\bar{x}:x_ix_o})^{-1} \cdot\cosh(\Delta\psi-\Delta\psi_i)]^{-1} \quad (41)$$

and the shape will depend on the ratio between the heights of the outer and inner peaks and on the fraction of voltage lying between the inner site and outer peak ("voltage seen in jumping out").

The high concentration limit for the 3*B*2*S* model, on the other hand is given by

$$J_x = \frac{2\sinh\left(-\frac{\Delta\psi}{2}\right)}{C_x} \cdot \frac{p_{\bar{x}}}{k_{x_i x_i}} \quad C_x \to \infty \ (3B2S) \qquad (42)$$

and behaves like a single-barrier step.

The same behavior is characteristic of the 3*B*4*S*′ model which also approaches a single-barrier behavior at high concentrations (Hägglund et al., 1982).

At *low concentrations* all three models (3*B*2*S*, 3*B*4*S*′, 3*B*4*S*″) approach the same limiting behavior (Eisenman et al., 1980; Hägglund et al., 1982)

$$J_x = C_x \cdot 2\sinh\left(-\frac{\Delta\psi}{2}\right)\left[\frac{1}{p_{\bar{x}}} + \frac{\cosh(\Delta\psi - \Delta\psi_0)}{p_{\bar{x}:}}\right]^{-1}$$
$$C_x \to 0. \qquad (43)$$

The shape in this limit depends on the ratio between the heights of the outer and inner peaks and on the fraction of the voltage lying between the outer peak and the aqueous solution ("voltage seen in jumping in").

Flux Ratio Exponent

The coupling between unidirectional fluxes in a channel with single filing properties was first discovered by Hodgkin and Keynes (1955). The phenomenon is usually demonstrated with the help of tracer fluxes, and a measure of their deviation from independence is given by the value of the flux ratio exponent in the equation

$$\frac{\vec{J}_x}{\overleftarrow{J}_x} = \left[\frac{C_x'}{C_x''}\exp(-\Delta\psi)\right]^n \qquad (44)$$

where $\vec{J}_x$, $\overleftarrow{J}_x$ are unidirectional fluxes. It was shown by Heckmann (1965*b*) that the quantity n is also equal to the ratio between the permeability of a substance and that of its tracer, which is a more suitable form for deriving expressions for n in terms of the parameters of barrier models. If, instead of permeabilities, we use conductances and define the conductance G_y^o of a tracer Y of X as

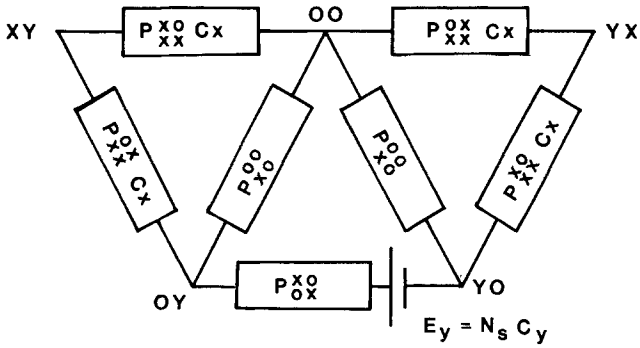

Fig. 8. Equivalent circuit diagram for the tracer conductance G_y^o when species X is at equilibrium. The circuit diagram is derived from the state diagram of Fig. 3 by open circuiting those elements which contain two (or more) tracer ions (Y) while short circuiting those elements which contain no tracer ions (Y), (*see* Sandblom et al. (1982) for development of the network theory)

$$G_y^o = \left(\frac{J_y}{\Delta\psi}\right)_{J_x = 0} \qquad (45)$$

then the flux ratio exponent is given by

$$n = \frac{G_x^o}{G_y^o} \cdot \frac{C_y}{C_x} \qquad (46)$$

where C_x, C_y are the concentrations of the substance and its tracer.

The conductance G_y^o can be derived using a circuit representation analogous to the representation of G_x^o in Fig. 5. The circuit corresponding to G_y^o is obtained from the steady-state diagram of Fig. 3 by taking into account that the upper part of the state diagram (species X) is virtually short circuited in comparison with the lower part of the state diagram (the tracer Y) due to the low concentration of the tracer (Sandblom et al., 1982). The representation of G_y^o is therefore given by the circuit in Fig. 8 from which a straightforward use of circuit theory gives the following expression for G_y^o

$$G_y^o = N_s C_y \left[\frac{1}{p_{xo}^{ox}} + \frac{2}{p_{ox}^{oo} + \frac{1}{2}p_{xx}^{xo} C_x}\right]^{-1}. \qquad (47)$$

N_s, the zero occupancy probability is not affected by the presence of a tracer and is therefore still given by Eq. (31). The ratio between G_y^o/C_y (Eq. (47)) and G_x^o/C_x (Eq. (37b)) gives the desired expression for n

$$n = \left[\frac{1}{p_{xo}^{ox}} + \frac{2}{p_{ox}^{oo} + p_{xx}^{xo} C_x}\right]^{-1}\left[\frac{1}{p_{xo}^{ox}} + \frac{2}{p_{ox}^{oo} + \frac{1}{2}p_{xx}^{xo} C_x}\right]. \qquad (48)$$

The value of n lies in the interval $1 < n < 2$, and at high concentrations it approaches the limit

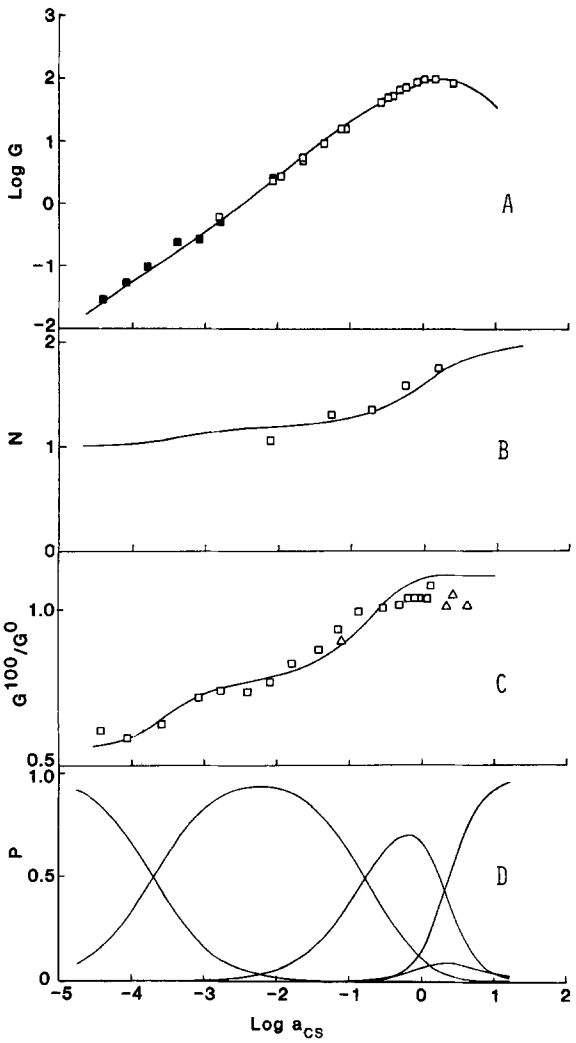

Fig. 9. The logarithm of $G^o_{Cs}(A)$, the flux ratio exponent (B), the voltage dependence $G^{100}_{Cs}/G^o_{Cs}(C)$ and the occupancy number at equilibrium (D) are plotted *vs.* the logarithm of the cesium activity. The experimental data have been published elsewhere (*see* text), and the curves represent a best fit of the data to the 2*B*4*S* model

$$n=\left[\frac{1}{p^{ox}_{xo}}+\frac{2}{p^{xo}_{xx}C_x}\right]^{-1}\left[\frac{1}{p^{ox}_{xo}}+\frac{4}{p^{xo}_{xx}C_x}\right] \quad C_x\to\infty. \tag{49}$$

If the peak parameters are constants (as they would be for a 3*B*2*S* model) the value of n is seen to decline towards unity. However, if we expand the lumped parameters in Eq. (49) with the aid of Table 1 we get

$$n=\left[\frac{1}{p_{x_o\bar{x}x_o}}+\frac{2}{p_{\bar{x}:x_ix_o}}\right]^{-1}\left[\frac{1}{p_{x_o\bar{x}x_o}}+\frac{4}{p_{\bar{x}:x_ix_o}}\right]$$
$$C_x\to\infty \tag{50}$$

a value which remains constant at high concentrations. Since available data for the flux ratio exponent for gramicidin A channels all indicate that n reaches a plateau at high concentrations, it seems as if the 3*B*4*S*" model may be an adequate model for gramicidin channels.

Equation (48) can be written in terms of the parameters P of Eq. (37a)

$$n=\left[\frac{1}{P_1'+2P_2'C_x+P_3'C_x^2}+\frac{2}{P_1''+P_2''C_x+P_3''C_x^2}\right]^{-1}$$
$$\cdot\left[\frac{1}{P_1'+2P_2'C_x+P_3'C_x^2}\right.$$
$$\left.+\frac{2}{P_1''+\frac{1}{2}P_2''C_x+\frac{1}{2}P_3''C_x^2+\frac{1}{2}p_{\bar{x}:x_o}C_x}\right] \tag{51}$$

and it is seen that the flux ratio exponent n contains all the lumped P parameters of the conductance expression (37b) and, in addition, an intrinsic peak parameter $p_{\bar{x}:x_o}$. Since it depends only on the peaks, the value of n at a particular concentration is completely independent of the ion occupancy.

Experimental Determinations of the Parameters

To illustrate how, in principle, one can use the 3*B*4*S*" model to interpret the combined electrical and flux behavior over the full range of concentrations, we present an analysis for Cs.

The measurements of G^o_x and n described in this paper are equilibrium measurements and if the concentrations on the two sides of the membrane are held equal, the voltage across the membrane must be zero. Under these circumstances the measured parameters are independent of the distribution of the electric field and hence also of the barrier shapes and are therefore only dependent on the levels of the peaks and of the wells.

Equation (37) indicates that the peak parameters are uniquely determined from a G^o_x measurement with the exception of the parameters $p_{\bar{x}:x_o}$ and $p_{\bar{x}:x_i}$ which appear as a sum ($=P_2''$). However, in the expression for n (Eq. (51)) they appear with different coefficients

$$(p_{\bar{x}:x_o}+\tfrac{1}{2}p_{\bar{x}:x_i})C_x$$

and hence a combination of G^o_x and n is sufficient to determine all of the peak parameters.

Figure 9*a* contains data on G^o_{Cs} previously published for glycerol monooleate (GMO)/hexdecane (Eisenman et al., 1978, unfilled squares) and noise measurements (E. Neher, G. Eisenman and J. Sandblom, *unpublished*,

filled squares) in GMO/decane with 9 mM $MgSO_4$ at pH 5–6. Figure 9*b* shows a set of experimental data for the flux ratio exponent as a function of concentration measured for Cs by Andersen and Procopio (1979 and personal communication) in gramicidin A channels in DPPC bilayers. The experimental values are seen to approach a constant level of 2 at high concentrations from which we conclude that $P_3' \ll P_3''$ (*see* Eq. (51)), i.e., that the middle barrier is small compared to the outer barriers. If we assume this inequality to hold for all concentrations we can set $P_1' \approx P_2' \approx P_3' \approx \infty$ and we are left with four peak parameters to determine.

The two voltage independent quantites n and G_x^o contain eight parameters together, the four peak parameters and the four K-parameters appearing in Eq. (37) for G_x^o. The conductances at low voltage (50 mV) are first used to determine the K_1, K_2, K_3, K_4, P_1'', P_2'' and P_3''. We next use Andersen's flux ratio exponent data to fix the separate values of the two intrinsic peak parameters, $p_{\bar{x}:x_i}$ and $p_{\bar{x}:x_o}$, which appear as a sum $=P_2''$. Figure 9*a* and *b* show the best fit of Eqs. (37) and (51) (with $P_1' \approx P_2' \approx P_3' \approx \infty$) to the experimental data for n and G_x^o. The parameters extracted from the best fit are given in Fig. 10.

The occupancies calculated on the basis of the determined K-parameters are shown in Fig. 9*d*.

Whereas the peak parameters are completely determined from n and G_x^o, we need additional measurements to determine the individual binding constants contained in the K-parameters. For this we need to determine the voltage dependence of the K-parameters and which will also yield the electric field distribution across the channel (i.e., the shape of the barriers). For the particular case of a symmetrical channel there are two "shape" factors, the location of the inner site (f_{oi}) and the location of the outer peak (f_o). In addition there are four more parameters to be determined from the voltage dependence of the parameters since the four K-parameters determined from the G_x^o measurement contain eight binding constants.

In order to extract the six additional parameters (2 shape factors + 8 binding constants − 4 K parameters) from their voltage dependence, it is sufficient to fix the voltage at one level and then determine the conductance at this level for different concentrations.

Figure 9*c* shows the experimental values for

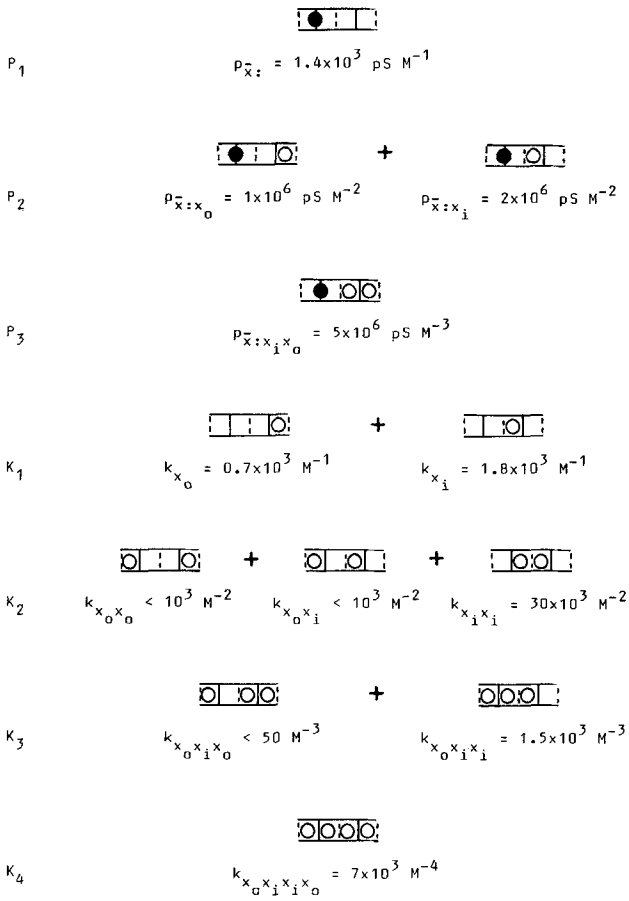

Fig. 10. The parameters consisting of intrinsic peak parameters and binding constants which have been extracted from the best fit of the 2*B*4*S* model to the experimental data of Fig. 9 are shown. The lumped parameters (P_1, P_2, P_3, K_1, K_2, K_3, K_4) determined from G_{Cs}^o (Fig. 9*a*) are indicated to the left in the figure and the individual (intrinsic) parameters contained in the lumped parameters are shown in the corresponding rows

such a measurement where the conductance is measured at 100 mV and divided by G_x^o. The published data of Eisenman et al. (1982) (open squares) and those of Hladky, Urban and Haydon (1979) (triangles) are used. The theoretical curve in Fig. 9*c* is generated by dividing the value of G_x^{100} calculated from Eq. (39) by the value of G_x^o calculated from Eq. (37). The values of K_1, K_2, K_3, K_4, P_1'', P_2'', P_3'', were used as fixed values in fitting the current voltage data and the remaining individual parameters were varied to give the best fit to the data. The set of individual parameters extracted from a fit to the experiments in Fig. 9 are summarized in Fig. 10.

A best fit to the I–V data (Fig. 9*c*) requires that the contributions to the K-values of cer-

tain binding constants are reduced to a minimum. The final values of these parameters are indicated by an upper estimate, based on the uncertainty of the curve-fitting procedure.

Discussion

A. Physical Interpretations of Models using Experimental Data

We have shown that by fitting a given barrier model to experimental data it is possible to extract a set of parameters which consist of intrinsic parameters or in some cases (e.g., a G_x^o measurement) lumped parameters. In principle a complete current-voltage behavior over the whole concentration range is sufficient to characterize all the intrinsic parameters of the $3B4S''$ model for a single permeable species. The only exception is the binding constant $k_{x_o x_i}$ which consists of the sum $k_{x_i x_o} + k_{x_o x_i}$ and which when the potential drop across the outer sites is zero cannot be separated by any measurement described in this paper. We therefore treat this parameter as a lumped constant describing the $x_o x_i$-binding.

Since each intrinsic parameter describes a combined energy level we can interpret physically the meaning of each parameter from the scheme shown in Fig. 10. The parameter values indicated in the figure were obtained from the fit of the $2B4S$ model to CsCl, the curves of which are shown in Fig. 9.

The lower four rows in the figure correspond to the four occupancy levels and the three upper rows correspond to the three peak energy levels which combine a peak with either zero, one or two ions bound to the indicated sites.

Some preliminary conclusions about the physical nature of the permeation process can now be drawn from the values of the parameters.

Firstly, it can be seen that each loading step reduces the constants of binding, for if the binding of an ion would be completely independent of loading then the combined parameter should be equal to the *product* of all the corresponding individual binding constants, for instance

$$k_{x_i x_i} = k_{x_i} \cdot k_{x_i} = 1800^2 = 3.64 \times 10^6 \text{ M}^{-2}$$

The actual value of $k_{x_i x_i}$ is much smaller than predicted from complete independence, and this applies to all steps. Each ion loading is therefore opposed by repulsive forces, which is to be expected from the electrostatic interactions with the ions occupying the sites.

An interesting result, however, is the preferred loading of the inner sites over the outer sites, which is deduced from the rows of double ($k_{x_i x_i} \gg k_{x_o x_i}$, $k_{x_o x_o}$) and triple occupancies ($k_{x_i x_i x_o} \gg k_{x_o x_i x_o}$). Since electrostatic repulsion forces are much stronger in the former case, the result must be interpreted as a cooperative phenomenon, possibly a conformational change produced by moving ions into the inner part of a channel. A conformational change which is stabilized by ion occupancy is also suggested by the increase in lifetime with ion concentration (Kolb & Bamberg, 1977).

B. Relationships to Rate Constants

The theory and its application to experimental data have been based on the use of peak parameters and binding constants. The advantage of using these instead of rate constants is, firstly, that the peak and well parameters incorporate the equations of detailed balance (microscopic reversibility) and therefore represent a set of independent parameters of the system. Secondly, the energies of wells and peaks represent energies of channel *states* and therefore directly yield the energies of interactions between ions occupying the channel as well as the energies of ion-ligand interactions in the channel.

The rate constants, on the other hand, are advantageous for comparing barrier heights and can be obtained by combining the peak parameters with the binding constants of the neighboring wells. Table 2 gives the rate constants for jumping out of the channel based on the numbers in Fig. 10.

The exit rate for jumping out from an inner site is seen to be greatly diminished when the adjacent inner site is occupied and enhanced when the opposite outer site is occupied. This again reflects the stabilizing effect of the doubly occupied inner sites and the repulsive electrostatic effects produced by ions occuping the outer sites.

The net entrance rate, i.e., the rate at which ions move from the aqueous solution to the inner site which includes crossing the outer well and outer barrier, is seen to be relatively unaffected by ion loading, which indicates that the energy of the entry step, the partial dehy-

Table 2.

Exit rate[a] (pS)	Occupancy	Entry rate[a] ($pS\,M^{-1}$)
$\upsilon_{x_i}^{x_o}=\frac{p_{\bar{x}:}}{k_{x_i}}=0.8$	Empty	$\upsilon^{x_i}=p_{\bar{x}:}=1.4\cdot10^3$
$\upsilon_{x_ix_o}^{x_ox_o}=\frac{p_{\bar{x}:x_o}}{k_{x_ix_o}}>2\cdot10^3$	Outer site	$\upsilon_{x_o}^{x_ix_o}=\frac{p_{\bar{x}:x_o}}{k_{x_o}}=2.9\cdot10^3$
$\upsilon_{x_ix_i}^{x_ix_o}=\frac{p_{\bar{x}:x_i}}{k_{x_ix_i}}=33$	Inner site	$\upsilon_{x_i}^{x_ix_i}=\frac{p_{\bar{x}:x_i}}{k_{x_i}}=0.56\cdot10^3$
$\upsilon_{x_ox_ix_i}^{x_ox_ix_o}=\frac{p_{\bar{x}:x_ix_o}}{k_{x_ox_ix_i}}=3.3\cdot10^3$	Outer+inner site	$\upsilon_{x_ox_i}^{x_ox_ix_i}=\frac{p_{\bar{x}:x_ix_o}}{k_{x_ix_o}}>5\cdot10^3$

[a] The constants are converted from pS to sec^{-1} by multiplication with the factor $10^{-12}\times RT/Fe=1.6\times10^5$.

dration of the ions, is independent of electrostatic repulsive forces from the ions occupying the sites.

This work was supported chiefly by grant No. B81-14X-04138-06B from the Swedish Medical Research Council and partially by the U.S. Public Health Service (GM 24749) and the U.S. National Science Foundation (PCM 7620605).

References

Andersen, O.S. 1982*a*. Ion movement through gramicidin A channels. Single channel measurements at very high potentials. *Biophys. J. (submitted)*

Andersen, O.S. 1982*b*. Ion movement through gramicidin A channels. Interfacial polarization effects on single-channel current measurements. *Biophys. J. (submitted)*

Bamberg, E., Läuger, P. 1977. Blocking of the gramicidin channel by divalent cations. *J. Membrane Biol.* **35**:351–375

Chizmadjev, Y.A., Aityan, S.K. 1977. Ion transport across sodium channels in biological membranes. *J. Theor. Biol.* **64**:429–453

Eisenman, G., Hägglund, J., Sandblom, J., Enos, B. 1980. The current-voltage behavior of ion channels: Important features of the energy profile of the gramicidin channel induced from the conductance-voltage characteristic in the limit of low ion concentrations. *Upsala J. Med. Sci.* **85**:247–257

Eisenman, G., Sandblom, J., Hägglund, J. 1982. Electrical behavior of single-filing channels. *In*: Structure and Function in Excitable Cells. W. Adelman, D. Chang, R. Leuchtag, and I. Tasaki, Editors. Plenum, New York (*in press*)

Enos, B.E., Peskoff, A. 1979. Electrostatic calculations for an ion channel in contact with an electrolyte solution. *Biophys. J.* **25**:214a

Finkelstein, A., Andersen, O.S. 1981. The gramicidin A channel: A review of its permeability characteristics with special reference to the single-file aspect of transport. *J. Membrane Biol.* **59**:155–177

Hägglund, J.V., Eisenman, G., Sandblom, J. 1982. Single salt behavior of a symmetrical 4-site channel with barriers at its middle and ends. *Bull. Math. Biol. (submitted)*

Hägglund, J., Enos, B., Eisenman, G. 1979. Multi-site, multi-barrier, multi-occupancy models for the electrical behavior of single filing channels like those of gramicidin. *Brain Res. Bull.* **4**:154–158

Heckmann, K. 1965*a*. Zur Theorie der "single file"-Diffusion, I. *Z. Phys. Chem. (N.F.)* **44**:184–203

Heckmann, K. 1965*b*. Zur Theorie der "single file"-Diffusion, II. *Z. Phys. Chem. (N.F.)* **46**:1–25

Heckmann, K. 1968. Zur Theorie der "single file"-Diffusion, III. Sigmoide Konzentrationsabhängigkeit unidirectionaler Flüsse bei "single file"-Diffusion. *Z. Phys. Chem. (N.F.)* **58**:206–219

Hille, B. 1978. Ionic channels in excitable membranes. Current problems and biophysical approaches. *Biophys. J.* **22**:283–294

Hille, B., Schwartz, W. 1978. K channels of nerve and muscle: Single-file, multi-ion pores. *J. Gen. Physiol.* **72**:409–422

Hladky, S.B., Urban, B.W., Haydon, D.A. 1979. Ion movements in pores formed by gramicidin A. *In*: Membrane Transport Processes. C. Stevens, R. Tsien and W. Chandler editors. Vol. 3, pp. 89–103. Raven Press, New York

Hodgkin, A.L., Keynes, R.D. 1955. The potassium permeability of a giant nerve fibre. *J. Physiol. (London)* **128**:61–88

Kolb, H.A., Bamberg, E. 1977. Influence of membrane thickness and ion concentration on the properties of the gramicidin channel. Autocorrelation, spectral power density, relaxation and single-channel studies. *Biochim. Biophys. Acta* **464**:127–141

Levitt, D.G. 1978. Electrostatic calculations for an ion channel. II. Kinetic behavior of the gramicidin A. channel. *Biophys. J.* **22**:221–248

Levitt, D.G., Elias, S.R., Hautman, J.M. 1978. Number of water molecules coupled to the transport of Na^+, K^+, and H^+ via gramicidin, nonactin or valinomycin. *Biochim. Biophys. Acta* **512**:436–451

Neher, E., Sandblom, J., Eisenman, G. 1978. Ionic selectivity, saturation, and block in gramicidin A channels.

II. Saturation behavior of single channel conductance and evidence for the existence of multiple binding sites in the channel. *J. Membrane Biol.* **40**:97–116

Procopio, J., Andersen, O.S. 1979. Ion tracer fluxes through gramicidin A modified lipid bilayers. *Biophys. J.* **25**:8*a*

Rosenberg, P.A., Finkelstein, A. 1978. Interaction of ions and water in gramicidin A channels. Streaming potentials across lipid bilayer membranes. *J. Gen. Physiol.* **72**:327–339

Sandblom, J., Eisenman, G., Neher, E. 1977. Ionic selectivity, saturation and block in gramicidin A channels: I. Theory for the electrical properties of ion selective channels having two pairs of binding sites and multiple conductance states. *J. Membrane Biol.* **31**:383–417

Sandblom, J., Ring, A., Eisenman, G. 1982. Linear network representation of multistate models of transport. *Biophys. J.* **38**:95–104

Schagina, L.V., Grinfeldt, A.E., Lev, A.A. 1978. Interaction of cation fluxes in gramicidin A channels in lipid bilayer membranes. *Nature (London)* **273**:243–244

Urban, B.W., Hladky, S.B. 1979. Ion transport in the simplest single file pore. *Biochim Biophys. Acta* **554**:410–429

Urry, D.W., Venkatachalam, C.M., Spisni, A., Bradley, R.J., Trapane, T.L., Prasad, K.U., 1980. The malonyl gramicidin channel: NMR-derived rate constants and comparison of calculated and experimental single-channel current *J. Membrane Biol.* **55**:29–51

Received 2 March 1982